

# Catalytic Four-Electron Reduction of O<sub>2</sub> via Rate-Determining Proton-Coupled Electron Transfer to a Dinuclear Cobalt- $\mu$ -1,2-peroxo Complex

Shunichi Fukuzumi,<sup>\*,†,‡</sup> Sukanta Mandal,<sup>‡,§</sup> Kentaro Mase,<sup>†</sup> Kei Ohkubo,<sup>†</sup> Hyejin Park,<sup>‡</sup> Jordi Benet-Buchholz,<sup>§</sup> Wonwoo Nam,<sup>\*,‡</sup> and Antoni Llobet<sup>\*,‡,§</sup>

<sup>†</sup>Department of Material and Life Science, Graduate School of Engineering, Osaka University, and ALCA, Japan Science and Technology Agency, Suita, Osaka 565-0871, Japan

<sup>‡</sup>Department of Bioinspired Science, Ewha Womans University, Seoul 120-750, Korea

<sup>§</sup>Institute of Chemical Research of Catalonia, Avinguda Països Catalans 16, E-43007 Tarragona, Spain

## Supporting Information

**ABSTRACT:** Four-electron reduction of O<sub>2</sub> by octamethylferrocene (Me<sub>8</sub>Fc) occurs efficiently with a dinuclear cobalt- $\mu$ -1,2-peroxo complex, **1**, in the presence of trifluoroacetic acid in acetonitrile. Kinetic investigations of the overall catalytic reaction and each step in the catalytic cycle showed that proton-coupled electron transfer from Me<sub>8</sub>Fc to **1** is the rate-determining step in the catalytic cycle.

The catalytic four-electron (4e<sup>-</sup>) reduction of O<sub>2</sub> to water has merited increasing attention because it is intrinsic to respiration<sup>1</sup> as well as fuel cell technology.<sup>2</sup> In fuel cells, the 4e<sup>-</sup> reduction of O<sub>2</sub> is catalyzed at the cathode by Pt impregnated in carbon.<sup>2,3</sup> The high loadings of this precious metal that are required to achieve appreciable activity have prompted the development of catalysts based on nonprecious metals such as Co, Cu, and Fe.<sup>4–7</sup> In addition to electrocatalytic reduction of O<sub>2</sub> with nonprecious metal complexes, homogeneous catalytic reduction of O<sub>2</sub> by one-electron (1e<sup>-</sup>) reductants such as ferrocene (Fc) derivatives has provided mechanistic insight into the key question: How can the two-electron (2e<sup>-</sup>) versus 4e<sup>-</sup> reduction of O<sub>2</sub> be controlled by metal complexes?<sup>8–13</sup> The key intermediate for the catalytic 4e<sup>-</sup> reduction of O<sub>2</sub> is usually regarded to be a dinuclear metal–peroxo complex, which is further reduced to water. However, there has been no study of the electron-transfer (ET) reduction of isolated dinuclear metal–peroxo complexes with structures established by X-ray crystallography. Thus, the exact role of the dinuclear complex in the catalytic 4e<sup>-</sup> reduction of O<sub>2</sub> has yet to be uncovered.

We report that a dinuclear cobalt- $\mu$ -1,2-peroxo complex with bis(pyridyl)pyrazolate (bpp) and terpyridine (trpy) ligands, [Co<sup>III</sup><sub>2</sub>(trpy)<sub>2</sub>( $\mu$ -bpp)( $\mu$ -1,2-O<sub>2</sub>)]<sup>3+</sup> (**1**), catalyzes the 4e<sup>-</sup> reduction of O<sub>2</sub> by Fc derivatives in the presence of trifluoroacetic acid (TFA) in MeCN at 298 K. The structure of **1** was successfully determined by X-ray crystallography. Kinetic studies of the overall catalytic cycle and each step in the catalytic cycle enabled us to show for the first time that proton-coupled electron transfer (PCET) reduction of **1** is the rate-determining step in the overall catalytic 4e<sup>-</sup> reduction of O<sub>2</sub>.

Complex **1** was synthesized by the reaction of Co(trpy)Cl<sub>2</sub> with bpp under O<sub>2</sub> in methanol [Figure 1; also see the

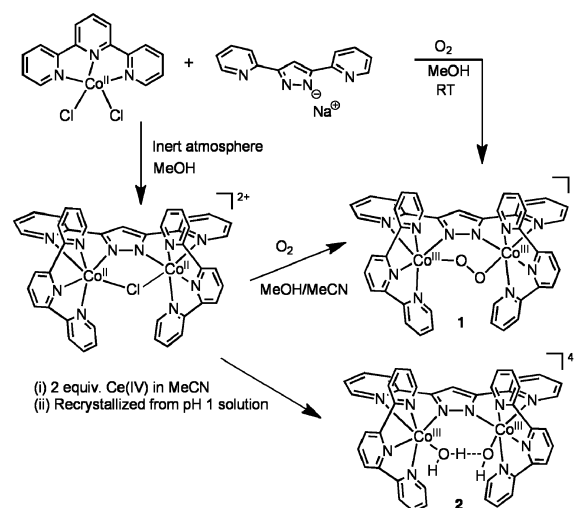


**Figure 1.** Syntheses of complexes **1** and **2**.

Experimental Section in the Supporting Information (SI)]. The aqua–hydroxo complex **2** was obtained by oxidation of [Co<sup>II</sup><sub>2</sub>(trpy)<sub>2</sub>( $\mu$ -bpp)( $\mu$ -Cl)](PF<sub>6</sub>)<sub>2</sub> with cerium(IV) ammonium nitrate (Figure 1; also see the SI). Both **1** and **2** were well-characterized by spectroscopic methods (Figures S3–S6 in the SI) and X-ray crystallography (Figure 2). The X-ray structure of **1** (Figure 2a) shows that the peroxo ligand is coordinated to the two Co<sup>III</sup> ions in a  $\mu$ -1,2 fashion. The O–O bond distance, 1.397(2) Å, is typical for dinuclear Co–peroxo complexes.<sup>14</sup> The structure of **2** (Figure 2b) shows that the aqua and hydroxo ligands are coordinated to the two Co<sup>III</sup> ions and share a H atom. The O–O distance of 2.415 Å is long enough to accommodate the H atom.

The 4e<sup>-</sup> reduction of O<sub>2</sub> by octamethylferrocene (Me<sub>8</sub>Fc) occurred with a catalytic amount of **1** in the presence of TFA in MeCN at 298 K (Figure 3a), with complete conversion of

Received: April 17, 2012

Published: June 1, 2012

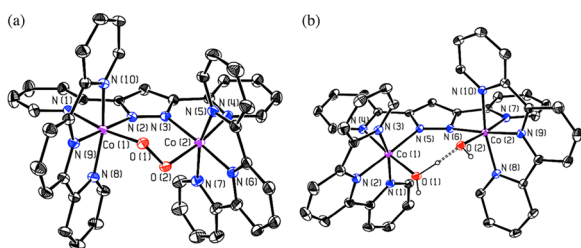


**Figure 2.** ORTEP plots (50% probability) of the crystal structures of the cationic parts of (a) **1** and (b) **2**. H atoms, counteranions, and solvent molecules of crystallization have been omitted for clarity.

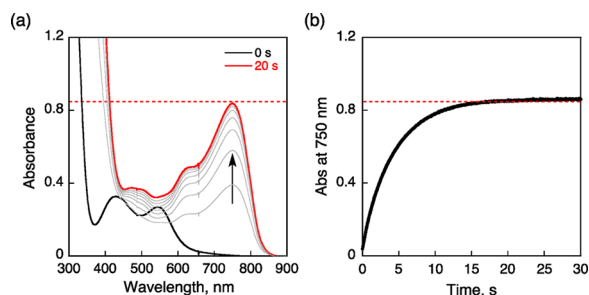
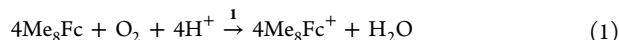


**Figure 3.** (a) Absorption spectral changes in the  $4e^-$  reduction of  $O_2$  by  $Me_8Fc$  (2 mM) catalyzed by **1** (25  $\mu M$ ) in the presence of TFA (50 mM) in  $O_2$ -saturated MeCN at 298 K. The black and red lines show the spectra before and after addition of TFA, respectively. The dotted line is the absorbance at 750 nm due to 2 mM  $Me_8Fc^+$ . (b) Time profile of the absorbance at 750 nm due to  $Me_8Fc^+$ .

$Me_8Fc$  to  $Me_8Fc^+$  ( $\lambda_{max} = 750$  nm,  $\epsilon = 410$   $M^{-1} cm^{-1}$ ). Iodometric titrations confirmed that no  $H_2O_2$  was formed after the reaction was complete (Figure S7). Thus, **1** catalyzes the  $4e^-$  reduction of  $O_2$  by  $Me_8Fc$  in the presence of TFA in MeCN:



The time profile in Figure 3b indicates that this process proceeds in a single step rather than by stepwise reduction of  $O_2$  to  $H_2O_2$  and then to  $H_2O$ . When **1** was replaced by **2**, the  $4e^-$  reduction of  $O_2$  by  $Me_8Fc$  occurred at the same rate (Figure S8).

The formation of  $Me_8Fc^+$  obeyed pseudo-first-order kinetics (Figure 3b). The pseudo-first-order rate constant ( $k_{obs}$ ) increased linearly with increasing concentration of **1** (Figure 4a) but did not depend on the  $O_2$  concentration (Figure 4b). Thus, the kinetic equation is

$$\frac{d[Me_8Fc^+]}{dt} = k_{cat}[Me_8Fc][1] \quad (2)$$

where  $k_{cat}$  is the second-order rate constant for the catalytic  $4e^-$  reduction of  $O_2$  by  $Me_8Fc$ .  $k_{cat}$  increased with increasing TFA concentration with a nonzero intercept (Figure 5a). The  $4e^-$  reduction of  $O_2$  by dexamethylferrocene ( $Fc^*$ ) catalyzed by **1** in the presence of TFA in MeCN at 298 K occurred more efficiently than that by  $Me_8Fc$  (Figure S9).<sup>15</sup>

The  $4e^-$  reduction of  $O_2$  requires the reduction of **1** by  $Me_8Fc$ . Thus, we examined the reduction of **1** by  $Me_8Fc$  in the absence and presence of TFA in deaerated MeCN. In the absence of TFA, no reduction of **1** by  $Me_8Fc$  was observed. In the presence of TFA, however, **1** was efficiently reduced by  $Me_8Fc$  (Figure 6a), as the absorption band at 545 nm due to **1** disappeared, accompanied by the appearance of the absorption

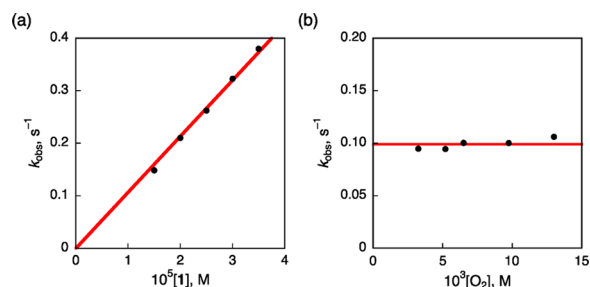


**Figure 4.** Plots of (a)  $k_{obs}$  vs  $[1]$  in  $O_2$ -saturated MeCN and (b)  $k_{obs}$  vs  $[O_2]$  with  $[1] = 25$   $\mu M$  for the  $4e^-$  reduction of  $O_2$  by  $Me_8Fc$  (1.5 mM) in the presence of TFA (50 mM) in MeCN.

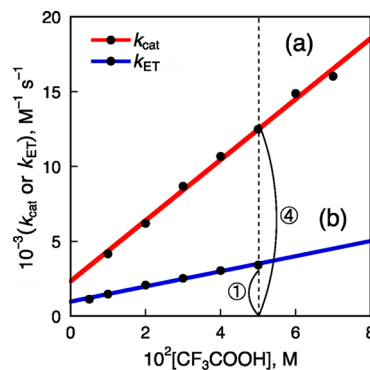


**Figure 5.** (a) Plot of  $k_{cat}$  vs TFA concentration for the catalytic  $4e^-$  reduction of  $O_2$  by  $Me_8Fc$  (1.5 mM) in  $O_2$ -saturated MeCN at 298 K. (b) Plot of  $k_{ET}$  vs TFA concentration for the reaction involving ET from  $Me_8Fc$  (1.5 mM) to **1** (25  $\mu M$ ) in deaerated MeCN at 298 K.

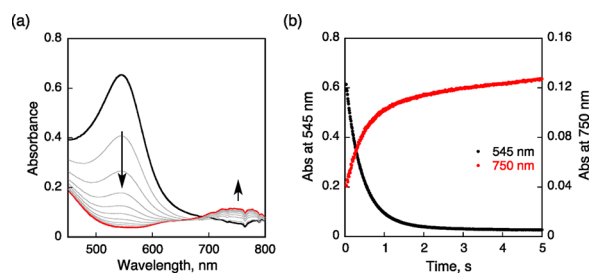
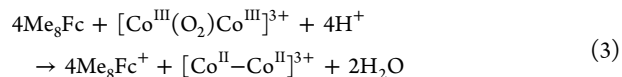


**Figure 6.** (a) Absorption spectral changes in the reduction of **1** (50  $\mu M$ ) by  $Me_8Fc$  (1.5 mM) in the presence of TFA (50 mM) in deaerated MeCN. (b) Time profiles of the absorbance at 545 nm due to decreasing **1** (black) and 750 nm due to increasing  $Me_8Fc^+$  (red).

band at 750 nm due to  $Me_8Fc^+$ . The decay rate of **1** coincided with the rate of formation of  $Me_8Fc^+$  (Figure 6b). The stoichiometry of the PCET reduction of **1** by  $Me_8Fc$  was determined to be



The ET from  $Me_8Fc$  to **1** in the presence of TFA obeyed pseudo-first-order kinetics (Figure S10a), and  $k_{obs}$  increased linearly with increasing  $[Me_8Fc]$  concentration (Figure S10b). Thus, the decay rate of **1** is given by

$$-\frac{d[1]}{dt} = \frac{1}{4} \frac{d[Me_8Fc^+]}{dt} = k_{ET}[1][Me_8Fc] \quad (4)$$

where  $k_{ET}$  is the second-order rate constant for ET from  $Me_8Fc$  to **1** in the presence of TFA. Because 4 equiv of  $Me_8Fc^+$  are

produced by ET from  $\text{Me}_8\text{Fc}$  to **1** in the presence of TFA, the decay rate of **1** is equal to one-fourth the formation rate of  $\text{Me}_8\text{Fc}^+$  (eq 4). The  $k_{\text{ET}}$  value increased linearly with increasing TFA concentration with a nonzero intercept (Figure 5b). The intercept corresponds to ET from  $\text{Me}_8\text{Fc}$  to **1**, which is followed by much faster PCET, and the linear dependence of  $k_{\text{ET}}$  on  $[\text{TFA}]$  suggests that initial ET from  $\text{Me}_8\text{Fc}$  to **1** is accelerated by the acid. Although no protonation of **1** by TFA was observed, as indicated by the absence of absorption spectral changes for **1** in the presence of TFA (Figure S11a), absorption spectral changes due to demetalation of **1** were observed in the presence of  $\text{HClO}_4$ , which is a much stronger acid than TFA (Figure S11b). Since  $k_{\text{ET}}$  increased linearly with increasing TFA concentration (Figure 5b), ET from  $\text{Me}_8\text{Fc}$  to protonated **1**, whose concentration is proportional to the TFA concentration, may be much faster than ET from  $\text{Me}_8\text{Fc}$  to **1**.

Comparison of  $k_{\text{cat}}$  and  $k_{\text{ET}}$  at various TFA concentrations (Figure 5) showed  $k_{\text{cat}}$  always to be 4 times as large as  $k_{\text{ET}}$ . This indicates that the PCET reduction of **1** by  $\text{Me}_8\text{Fc}$  is the rate-determining step in the overall catalytic cycle of the  $4e^-$  reduction of  $\text{O}_2$  by  $\text{Me}_8\text{Fc}$  in the presence of TFA in MeCN.

The  $k_{\text{ET}}$  values for ET from  $\text{Fc}^*$  to **1** in the presence of TFA in MeCN were also determined at 298 K and found to be  $\sim 10$  times larger than those for  $\text{Me}_8\text{Fc}$ , as expected given the lower  $1e^-$  oxidation potential of  $\text{Fc}^*$  ( $E_{\text{ox}} = -0.08$  V vs SCE) than of  $\text{Me}_8\text{Fc}$  ( $E_{\text{ox}} = -0.04$  V vs SCE).<sup>9</sup>

To confirm the thermodynamics of PCET from  $\text{Me}_8\text{Fc}$  to **1**, cyclic voltammograms (CVs) of **1** were measured in the absence and presence of TFA in MeCN (Figure 7). In the

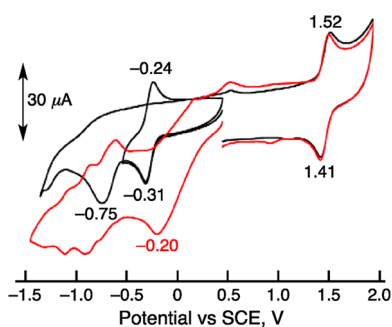


**Figure 7.** CVs of **1** in MeCN (1 mM) without TFA in the presence of 0.10 M TBAPF<sub>6</sub> (black) and with 2 mM TFA (red). Sweep rate = 100 mV s<sup>-1</sup>.

absence of TFA, the reversible  $\text{Co}^{\text{III}}_2/\text{Co}^{\text{III}}\text{Co}^{\text{II}}$  and  $\text{Co}^{\text{IV}}\text{Co}^{\text{III}}/\text{Co}^{\text{III}}_2$  couples were observed at  $E_{1/2} = -0.27$  and  $+1.47$  V vs SCE, respectively. The cathodic peak current observed at  $-0.75$  V corresponds to the reduction of  $\text{Co}^{\text{III}}\text{Co}^{\text{II}}$  to  $\text{Co}^{\text{II}}_2$ . However, this reduction was irreversible, probably because of the O–O bond cleavage in the dissociative ET reduction. In the presence of TFA, the reversible  $\text{Co}^{\text{IV}}\text{Co}^{\text{III}}/\text{Co}^{\text{III}}_2$  couple remained the same as that in the absence of TFA, whereas the  $\text{Co}^{\text{III}}_2/\text{Co}^{\text{III}}\text{Co}^{\text{II}}$  reduction peak was shifted in the positive direction.<sup>16</sup> This is consistent with the previous results for ET from  $\text{Me}_8\text{Fc}$  to **1**, as ET from  $\text{Me}_8\text{Fc}$  ( $E_{\text{ox}} = -0.04$  V vs SCE) to **1** ( $E_{\text{red}} = -0.27$  V vs SCE) is thermodynamically unfavorable but becomes energetically feasible in the presence of TFA.

Figure 8 shows a CV for aqua–hydroxo complex **2**. The two reversible couples observed at  $+0.31$  and  $-0.04$  V vs SCE correspond to the first  $1e^-$  reduction of **2** to the  $\text{Co}^{\text{III}}\text{Co}^{\text{II}}$  complex and the second  $1e^-$  reduction to the  $\text{Co}^{\text{II}}_2$  complex,

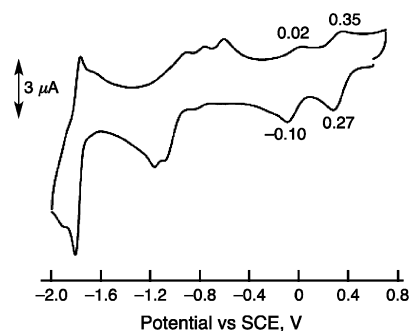


**Figure 8.** CV of **2** in MeCN (0.25 mM) in the presence of 0.10 M TBAPF<sub>6</sub>. Sweep rate = 100 mV s<sup>-1</sup>.

respectively. On the basis of the  $E_{\text{red}}$  values for **2**, ET from  $\text{Me}_8\text{Fc}$  to **2** to produce 2 equiv of  $\text{Me}_8\text{Fc}^+$  and the  $\text{Co}^{\text{II}}_2$  complex is thermodynamically feasible. In fact, ET from  $\text{Me}_8\text{Fc}$  to **2** occurs in two steps with rate constants of  $3.2 \times 10^5$  and  $1.6 \times 10^3$  M<sup>-1</sup> s<sup>-1</sup> for the first and second steps, respectively (Figures S12 and S13).

When **2** was reduced by 2 equiv of  $\text{Me}_8\text{Fc}$ , the peroxo complex was produced by the reaction of the reduced **2** with  $\text{O}_2$  (Figure 9a), as the absorption band due to **1** ( $\lambda_{\text{max}} = 545$  nm)

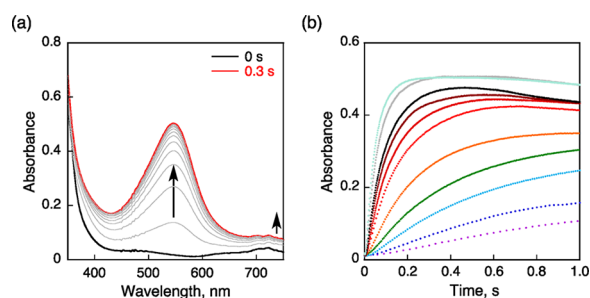
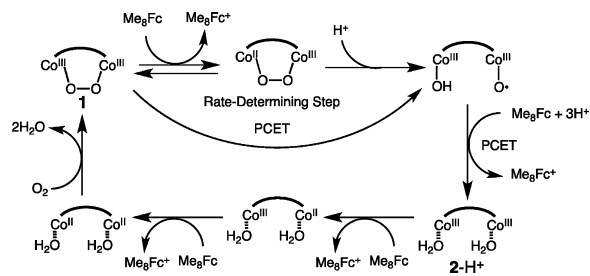


**Figure 9.** (a) Transient absorption spectral changes in the reaction of **2** (50 μM) with  $\text{Me}_8\text{Fc}$  (100 μM) in the presence of TFA (30 mM) in air-saturated MeCN. (b) Time profiles of the absorbance at 545 nm due to **1** in the reaction of **2** with  $\text{Me}_8\text{Fc}$  in the presence of various concentrations of TFA (100 μM to 30 mM) in air-saturated MeCN.

appeared together with that of  $\text{Me}_8\text{Fc}^+$  ( $\lambda_{\text{max}} = 750$  nm). The rate of formation of **1** increased with increasing TFA concentration (Figure 9b). Because the formation of **1** is much faster than the PCET reduction of **1**,<sup>17</sup> the formation of **1** in the catalytic cycle is not the rate-determining step.

The overall catalytic cycle is summarized in Scheme 1. When the reaction is started from peroxo complex **1**, **1** is reduced by PCET from  $\text{Me}_8\text{Fc}$ . Because the decay rate of **1** coincides with the rate of formation of 4 equiv of  $\text{Me}_8\text{Fc}^+$ , once **1** is reduced by PCET, the subsequent PCET processes should be much faster

#### Scheme 1



than the initial PCET process. The reduction of **1** by  $\text{Me}_3\text{Fc}$  can proceed via two pathways. One involves ET from  $\text{Me}_3\text{Fc}$  to **1** followed by protonation of the reduced **1**, which results in O–O bond cleavage. This is followed by rapid PCET to produce **2**. The other pathway involves coupling of the ET and the protonation, which occur in a concerted manner, since the PCET rate constant increases linearly with increasing TFA concentration (Figure 5). After **1** is converted to **2**, a fast ET reduction of **2** by  $\text{Me}_3\text{Fc}$  occurs, producing the  $\text{Co}^{\text{II}}$  complex, which reacts with  $\text{O}_2$  to regenerate **2**. When the reaction is started from **2**, **2** is converted rapidly to **1** by ET reduction of **2** and the reaction of the  $\text{Co}^{\text{II}}$  complex with  $\text{O}_2$ , both of which are much faster than the PCET reduction of **1**. Thus, the same catalytic rate is observed starting from **1** or **2**. Because the rate of formation of **1** from **2** with  $\text{Me}_3\text{Fc}$  increases with increasing TFA concentration (Figure 9), this process may also proceed via a PCET pathway, although the detailed mechanism has yet to be clarified.<sup>18</sup>

In conclusion, the  $4e^-$  reduction of  $\text{O}_2$  by  $\text{Me}_3\text{Fc}$  in the presence of TFA is efficiently catalyzed by the dinuclear  $\text{Co}^{\text{III}}$ –peroxy complex **1** as well as the aqua–hydroxo complex **2**. The X-ray structures of both **1** and **2** were successfully determined. Kinetic analyses of the overall catalytic process and each catalytic step revealed that PCET reduction of **1** is the rate-determining step in the overall catalytic cycle, which may not be the same as the natural process in respiration, however.

## ■ ASSOCIATED CONTENT

### Supporting Information

Experimental section, additional data, and complete ref 3. This material is available free of charge via the Internet at <http://pubs.acs.org>.

## ■ AUTHOR INFORMATION

### Corresponding Author

fukuzumi@chem.eng.osaka-u.ac.jp; wwnam@ewha.ac.kr; allobet@ICIQ-ES

### Notes

The authors declare no competing financial interest.

## ■ ACKNOWLEDGMENTS

This work was supported in part by Grants-in-Aid (20108010 to S.F. and 23750014 to K.O.) and a Global COE Program (to S.F.) from MEXT of Japan, by NRF/MEST of Korea through WCU Project R31-2008-000-10010-0 (to W.N.), and by MICINN of Spain (CTQ2010-21497 to A.L.).

## ■ REFERENCES

- (1) (a) Ferguson-Miller, S.; Babcock, G. T. *Chem. Rev.* **1996**, *96*, 2889. (b) Babcock, G. T.; Wikström, M. *Nature* **1992**, *356*, 301. (c) Babcock, G. T. *Proc. Natl. Acad. Sci. U.S.A.* **1999**, *96*, 12971. (d) Kaila, V. R. I.; Verkhovskiy, M. I.; Wikström, M. *Chem. Rev.* **2010**, *110*, 7062.
- (2) (a) Stambouli, A. B.; Traversa, E. *Renewable Sustainable Energy Rev.* **2002**, *6*, 295. (b) Marković, N. M.; Schmidt, T. J.; Stamenković, V.; Ross, P. N. *Fuel Cells* **2001**, *1*, 105. (c) Steele, B. C. H.; Heinzel, A. *Nature* **2001**, *414*, 345.
- (3) Borup, R.; et al. *Chem. Rev.* **2007**, *107*, 3904.
- (4) (a) Lee, K.; Zhang, L.; Zhang, J. In *PEM Fuel Cell Electrocatalysts and Catalyst Layers*; Springer: London, 2008; p 715. (b) Anson, F. C.; Shi, C.; Steiger, B. *Acc. Chem. Res.* **1997**, *30*, 437. (c) Wang, B. *J. Power Sources* **2005**, *152*. (d) Peljo, P.; Rauhala, T.; Murtomäki, L.; Kallio, T.; Kontturi, K. *Int. J. Hydrogen Energy* **2011**, *36*, 10033.

- (5) (a) Collman, J. P.; Devaraj, N. K.; Decréau, R. A.; Yang, Y.; Yan, Y.-L.; Ebina, W.; Eberspacher, T. A.; Chidsey, C. E. D. *Science* **2007**, *315*, 1565. (b) Collman, J. P.; Decréau, R. A.; Lin, H.; Hosseini, A.; Yang, Y.; Dey, A.; Eberspacher, T. A. *Proc. Natl. Acad. Sci. U.S.A.* **2009**, *106*, 7320. (c) Collman, J. P.; Ghosh, S.; Dey, A.; Decréau, R. A.; Yang, Y. *J. Am. Chem. Soc.* **2009**, *131*, 5034.

- (6) (a) Kadish, K. M.; Frémond, L.; Shen, J.; Chen, P.; Ohkubo, K.; Fukuzumi, S.; El Ojaimi, M.; Gros, C. P.; Barbe, J.-M.; Guillard, R. *Inorg. Chem.* **2009**, *48*, 2571. (b) Kadish, K. M.; Shen, J.; Frémond, L.; Chen, P.; Ojaimi, M. E.; Chkounda, M.; Gros, C. P.; Barbe, J.-M.; Ohkubo, K.; Fukuzumi, S.; Guillard, R. *Inorg. Chem.* **2008**, *47*, 6726. (c) Chen, W.; Akhigbe, J.; Brückner, C.; Li, C. M.; Lei, Y. *J. Phys. Chem. C* **2010**, *114*, 8633.

- (7) (a) Rosenthal, J.; Nocera, D. G. *Acc. Chem. Res.* **2007**, *40*, 543. (b) Dogutan, D. K.; Stoian, S. A.; McGuire, R.; Schwalbe, M.; Teets, T. S.; Nocera, D. G. *J. Am. Chem. Soc.* **2011**, *133*, 131. (c) Teets, T. S.; Cook, T. R.; McCarthy, B. D.; Nocera, D. G. *J. Am. Chem. Soc.* **2011**, *133*, 8114.

- (8) (a) Fukuzumi, S. *Prog. Inorg. Chem.* **2009**, *56*, 49. (b) Fukuzumi, S. *Bull. Chem. Soc. Jpn.* **1997**, *70*, 1. (c) Fukuzumi, S.; Ohkubo, K. *Coord. Chem. Rev.* **2010**, *254*, 372. (d) Fukuzumi, S. *Chem. Lett.* **2008**, *37*, 808.

- (9) (a) Fukuzumi, S.; Mochizuki, S.; Tanaka, T. *Inorg. Chem.* **1989**, *28*, 2459. (b) Fukuzumi, S.; Mochizuki, S.; Tanaka, T. *Inorg. Chem.* **1990**, *29*, 653. (c) Fukuzumi, S.; Mochizuki, S.; Tanaka, T. *J. Chem. Soc., Chem. Commun.* **1989**, 391.

- (10) (a) Fukuzumi, S.; Okamoto, K.; Gros, C. P.; Guillard, R. *J. Am. Chem. Soc.* **2004**, *126*, 10441. (b) Fukuzumi, S.; Okamoto, K.; Tokuda, Y.; Gros, C. P.; Guillard, R. *J. Am. Chem. Soc.* **2004**, *126*, 17059.

- (11) Halime, Z.; Kotani, H.; Li, Y.; Fukuzumi, S.; Karlin, K. D. *Proc. Natl. Acad. Sci. U.S.A.* **2011**, *108*, 13990.

- (12) (a) Peljo, P.; Murtomäki, L.; Kallio, T.; Xu, H.-J.; Meyer, M.; Gros, C. P.; Barbe, J.-M.; Girault, H. H.; Laasonen, K.; Kontturi, K. *J. Am. Chem. Soc.* **2012**, *134*, 5974. (b) Su, B.; Hatay, I.; Trojánek, A.; Samec, Z.; Khoury, T.; Gros, C. P.; Barbe, J.-M.; Daina, A.; Carrupt, P.-A.; Girault, H. H. *J. Am. Chem. Soc.* **2010**, *132*, 2655. (c) Hatay, I.; Su, B.; Li, F.; Méndez, M. A.; Khoury, T.; Gros, C. P.; Barbe, J.-M.; Ersoz, M.; Samec, Z.; Girault, H. H. *J. Am. Chem. Soc.* **2009**, *131*, 13453.

- (13) (a) Devoille, A. M. J.; Love, J. B. *Dalton Trans.* **2012**, *41*, 65. (b) Askarizadeh, E.; Yaghoob, S. B.; Boghaei, D. M.; Slawin, A. M. Z.; Love, J. B. *Chem. Commun.* **2010**, *46*, 710.

- (14) (a) Givaja, G.; Volpe, M.; Edwards, M. A.; Blake, A. J.; Wilson, C.; Schröder, M.; Love, J. B. *Angew. Chem., Int. Ed.* **2007**, *46*, 584. (b) Volpe, M.; Hartnett, H.; Leeland, J. W.; Wills, K.; Ogunshun, M.; Duncombe, B. J.; Wilson, C.; Blake, A. J.; McMaster, J.; Love, J. B. *Inorg. Chem.* **2009**, *48*, 5195.

- (15) When  $\text{Me}_3\text{Fc}$  was replaced by 1,1'-dimethylferrocene ( $\text{Me}_2\text{Fc}$ ), which is a weaker electron donor, no catalytic  $4e^-$  reduction of  $\text{O}_2$  occurred in the presence of TFA in MeCN because the ET reduction of **1** by  $\text{Me}_2\text{Fc}$  is thermodynamically unfavorable.

- (16) Although detailed analysis of the CV at negative potentials (ca.  $-1$  V) has yet to be performed, these peaks may correspond to the  $1e^-$  and  $2e^-$  reduction processes of  $\text{Co}^{\text{II}}$  complex **2**, which were observed in the CV of **2** (Figure 8), as the ET reduction of **1** in the presence of TFA results in O–O bond cleavage (eq 3).

- (17) The rate constant for the formation of **1** from **2** with  $\text{Me}_3\text{Fc}$  at  $[\text{TFA}] = 30$  mM (Figure 9b) was  $1.8 \times 10^5 \text{ M}^{-1} \text{ s}^{-1}$ , which is much larger than  $k_{\text{ET}}$  for the PCET reduction of **1** by  $\text{Me}_3\text{Fc}$  at the same TFA concentration ( $2.5 \times 10^3 \text{ M}^{-1} \text{ s}^{-1}$ ; Figure 5).

- (18) The rate constant of  $1.8 \times 10^5 \text{ M}^{-1} \text{ s}^{-1}$  for the formation of **1** from **2** with  $\text{Me}_3\text{Fc}$  at  $[\text{TFA}] = 30$  mM is much larger than that for the second-step ET from  $\text{Me}_3\text{Fc}$  to the  $\text{Co}^{\text{III}}\text{Co}^{\text{II}}$  complex ( $1.6 \times 10^3 \text{ M}^{-1} \text{ s}^{-1}$ ; Figure S13). Thus, the  $\text{Co}^{\text{III}}\text{Co}^{\text{II}}$  complex produced by the first-step ET from  $\text{Me}_3\text{Fc}$  to **2** may react with  $\text{O}_2$  by a PCET process prior to the second-step ET from  $\text{Me}_3\text{Fc}$  to the  $\text{Co}^{\text{III}}\text{Co}^{\text{II}}$  complex.